Article

Simultaneous Electrochemical Impedance Spectroscopy and Localized Surface Plasmon Resonance in a Microfluidic Chip: New Insights into the Spatial Origin of the Signal

Jaroslav Lazar, Ruben R. Rosencrantz, Lothar Elling, and Uwe Schnakenberg

Anal. Chem., **Just Accepted Manuscript** • DOI: 10.1021/acs.analchem.6b02307 • Publication Date (Web): 07 Sep 2016

Simultaneous Electrochemical Impedance Spectroscopy and Localized Surface Plasmon Resonance in a Microfluidic Chip: New Insights into the Spatial Origin of the Signal

Jaroslav Lazar[1], Ruben R. Rosencrantz[2], Lothar Elling[2], Uwe Schnakenberg[1]*

[1]Institute of Materials in Electrical Engineering 1, RWTH Aachen University, Sommerfeldstrasse 24, 52074 Aachen, Germany

[2] Laboratory for Biomaterials, Institute for Biotechnology and Helmholtz-Institute for Biomedical Engineering, RWTH Aachen University, Pauwelsstr. 20, 52074 Aachen, Germany

ABSTRACT: A novel flow-through sensor based on Electrochemical Impedance Spectroscopy (EIS) and Localized Surface Plasmon Resonance (LSPR) for analyzing biomolecular interactions under flow- and static conditions is developed and characterized. The sensor consists of a double-side gold coated perforated polycarbonate membrane as part of a microfluidic system made of poly(dimethylsiloxane) (PDMS). LSPR and EIS measurements are carried out simultaneously by applying media changes (water to NaCl solutions), unspecific adsorption of bovine serum albumin (BSA) or specific lectin binding on glycopolymer brushes. For BSA binding at the surface, EIS sensor signals mainly contain information from the binding activities at the sensor surface at low frequencies, whereas at high frequencies the change of bulk medium is the main contribution to the EIS signal. Here, the LSPR signal corresponds with EIS signal at high frequency. In contrast, in the case of lectin binding on glycopolymer brushes (3.4 nm thick), where the binding mainly takes place in the brush layer in the vicinity of the surface, LSPR data are correlated with the EIS signals at low frequencies. This leads to the conclusion that the origin of LSPR signals strongly depends on surface coverage and can be specified by simultaneously carrying out EIS measurements.

INTRODUCTION

Electrochemical Impedance Spectroscopy (EIS) is a standard measurement method for sensing of chemical binding effects on and at the vicinity of the electrodes. EIS is successfully used in applications where the characterization binding reactions between biomolecules at the electrode surfaces are of distinct interest. EIS has been applied e.g. in sensing of immunosensing protocols[1], DNA hybridization interactions[2,3], virus detection[4,5] and microbiological cell layers[6] as well as single cell experiments[7–9]. Technical applications, like coating or corrosion, have been successfully characterized by EIS technique[10]. EIS is known not only for its sensitivity against binding effects, but also against electrolytic conductivity and permittivity depending on the frequency range[11]. Furthermore, specific protein adsorption on surface assembled monolayers (SAMs) were studied in detail[12,13]. Recently, highly affine and specific multivalent glycopolymer brushes were synthesized on electrode surfaces[14]. The evaluation of lectin binding kinetics on different thick brush layers was investigated by carrying out EIS measurements in a microfluidic device with integrated interdigitated electrodes in a flow-over configuration[15].

Surface Plasmon Resonance (SPR) is an established and commercially available technique to measure especially protein binding kinetics. The Kretschmann configuration in flow-over mode is the most common one[16] reaching high resolution of 10^{-7} RIU (refractive index units)[17]. Unfortunately, in flow-over setups low flow rates are needed to achieve high efficiencies[18].

Furthermore, advanced systems have been developed based on nanohole arrays[19,20] and transmission mode[21]. The latter configuration benefits especially from the possibility of using a flow-through microfluidic setup which provides fast response times[22,23] and better efficiencies compared to the flow-over configuration[24]. Recently, a hand-held device was successfully developed[25].

The high potential of the nanohole perforated membranes for Localized Surface Plasmon Resonance (LSPR) sensors was demonstrated[26,27]. The nanohole arrays were realized not only using silicon nitride as membrane substrates with an regular arrangement of nanoholes in combination with a thin gold sensing layer on the top, but also as cheap perforated polymer substrates which are commonly used as filter membranes. Here, sufficient high sensitivities were reported[28–30] although the irregularly distributed nanoholes serving as resonators cannot achieve the resolution limits of regularly distributed arrays[31,32]. Nevertheless, using such a low-cost membrane the specific binding of a 11 kDa breast cancer marker[33] as well as the binding of lectin to glycopolymer brushes was reported [34].

The combination of EIS and LSPR has been investigated already in a flow-over configuration. For EIS interdigitated gold electrodes[35,36,36] or planar gold surface[37,38] were used, whereas LSPR was carried out in a Kretschmann configuration. Gold nanoparticles were used to enhance the simultaneous EIS and LSPR measurement[39]. Measurement of local surface charge density in LSPR signal was enabled by filtering and evaluating the influence of the

electrical perturbation on the optical signal[40,41]. This method is called electrochemical surface plasmon resonance [42,43,44].

Although the recent studies of LSPR-EIS combination show the innovation potential and new application possibilities, no comparison was carried out to the best of our knowledge until now to differentiate the origins and the contributions of the LSPR and EIS signals with respect to the kinetics of sensor surface coverage.

MATERIALS AND METHODS

Perforated polycarbonate filter membranes (ISOPORE HTTP01300 by Millipore, Merck Chemicals, Darmstadt, Germany) with randomly distributed nanoholes with diameters of 350 nm were used for all experiments. 70 nm thin gold layers were deposited on the both sides of the membrane using a Nordiko NS 2550 sputtering system (dc power of 250 W, pressure of 4.2 Pa, argon flow of 55 sccm). Gold-coated membranes were cut to 5 mm x 8 mm pieces which served as sensing areas for EIS and LSPR measurements (Figure 1).

Phosphate buffered saline (PBS) and NaCl were purchased from Sigma-Aldrich (Schnelldorf, Germany), bovine serum albumin (BSA) from Carl Roth (Karlsruhe, Germany), Lectins GS-II and ECL from VectorLabs (Burlingame, CA, US), HEPES-NaOH and $CaCl_2$ from Carl Roth (Karlsruhe, Germany). Lectin GS-II was handled in lectin binding buffer (10 mM HEPES-NaOH (pH 7.5), 150 mM NaCl, 0.1 mM $CaCl_2$). Deionized water (DI) was used to dilute NaCl and PBS buffer solutions. Only non-faradaic buffers were used, since stability difficulties occurred when ferri/ferrocyanide redox couple is added[45].

The gold membranes were consecutively cleaned in acetone, isopropanol, ethanol, and water. Finally, the membranes were cleaned by oxygen plasma treatment at 0.2 mbar for 5 min. Self-assembled initiator monolayers were formed on the gold surfaces by immersion of freshly prepared membranes into 2 mM solutions of bis[2-(2′-bromoisobutyryloxy)ethyl]disulfide (Sigma-Aldrich Schnelldorf, Germany) using ethanol as solvent at 30°C for 24 h. The membranes were rinsed with ethanol and then dried under a stream of nitrogen. PGlcNAcEMA brushes were prepared by SI-ATRP technique [34]. The initiator modified membrane was placed in a reactor and purged with nitrogen. 1.28 g (3.84 mmol) GlcNAcEMA [14] was placed into a reaction flask and stirred in 12 ml water/methanol = 1/3 (v/v) until complete dissolution. The solution was stirred under nitrogen for 20 min. Then, 120.04 mg (0.77 mmol) 2,2'-bipyridine, 30.44 mg (0.31 mmol) copper(I) chloride, and 17.17 mg (0.08 mmol) copper(II) bromide (all from Sigma-Aldrich (Schnelldorf, Germany)) were added and stirred until a homogeneous dark brown solution formed. The reactor was degassed with nitrogen by stirring for 20 min. The reaction mixture was transferred into the flask containing the membrane. The polymerization proceeded at room temperature for 120 minutes. Then, the membrane was thoroughly rinsed with water and water/methanol mixture and dried under nitrogen stream.

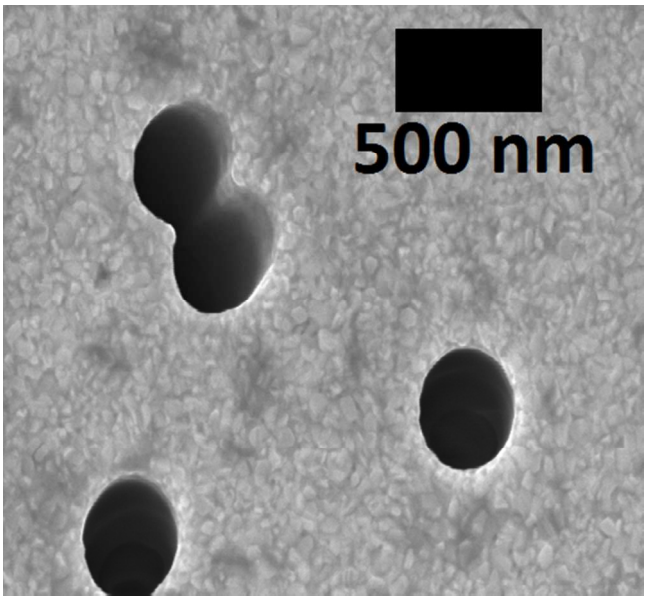

Figure 1: SEM image, top view of sputtered membrane showing nanoholes with straight inner walls.

The experimental setup for LSPR measurements was published elsewhere[33]. Briefly, a custom-made micro-chamber with a diameter of 1.5 mm and height of 100 µm was fabricated by using SU-8 (MicroChemicals, Ulm, Germany) masters and poly(dimethylsiloxane) (PDMS, Sylgard 184, Dow Corning, MI, USA) molding. A membrane was clamped in the cylindrical chamber. The chamber was connected to a custom-made microfluidic control station to supply the fluids consecutively (see Figure 2A). The inlets of the control station were connected to syringe pumps (Landgraf Laborsysteme HLL GmbH, Langenhagen, Germany) using Teflon tubes, see Figure 2B. The flow rate was adjusted to 0.5 ml/h for all experiments. In addition, the LSPR setup consists of a tungsten halogen lamp (SLS201(/M), Thorlabs, USA), focusing lenses, and a spectrometer (HR2000+, slit 50 µm, Ocean Optics, UK). The analysis of LSPR signals was carried out by calculating the barycentre of the transmission spectrum over time[33]. Barycentre shifts in horizontal direction in nm and vertical direction in intensity counted in auxiliary units as well as signal ratios were calculated.

For EIS measurements, the electrodes on both sides of the membrane were connected to a potentiostat/galvanostat/impedance analyzer (Versastat 3, Princeton Applied Research, Farnborough, Oak Ridge, TN, USA), as shown in Figure 2B. The frequency range for all EIS measurements was set from $f_{initial}$ = 100 kHz down to f_{final} = 1 Hz. The AC voltage was adjusted to V_{AC} = 10 mV and the DC voltage to the open-circuit potential (OCP), respectively, in order to stay in the linear region of the Butler-Volmer equation. LSPR and EIS measurements were carried out at least three times and simultaneously. EIS and LSPR data were finally edited in Origin 8.6 (OriginLab, MA, USA). During all experiments, the temperature was kept constant at 22 °C.

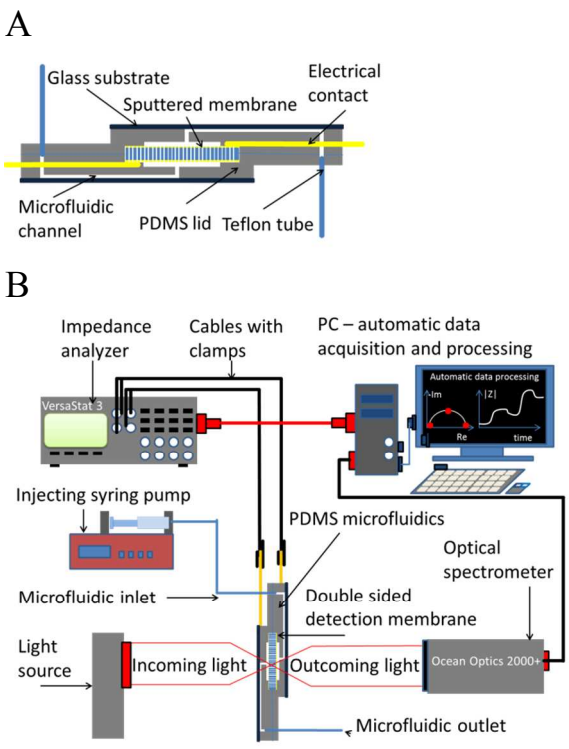

Figure 2: A) Scheme of the PDMS microfluidic system with clamped membrane. B) Schematic block diagram of the whole measurement setup. A) and B) not to scale.

RESULTS AND DISCUSSION

SYSTEM CHARACTERISATION

To determine the bulk refractive index resolution of the LSPR intensity signal five dilutions of NaCl in deionized water (DI) from 50.16 g/L to 231.6 g/L with corresponding refractive indices from 1.333 to 1.373 were purged through the membrane[46]. DI was used as reference solution. Figure 3A shows a linear dependency of the relative intensity and wavelength shifts of the spectral barycenter with respect to the refractive index. From this figure, a bulk refractive index sensitivities of 115.89 nm RIU^{-1} and 415.65 % RIU^{-1} were calculated. The averaged standard deviations of 0.015 nm and 0.032 % respectively at constant refractive index specified the resolutions of $1.32*10^{-4}$ RIU for the wavelength barycenter shift and $7.81*10^{-5}$ RIU for the relative intensity barycenter change, respectively. The 60 times lower resolution of the wavelength shift evaluation is caused by higher standard deviation compared to the relative intensity change. Therefore, only relative intensity barycenter changes were considered in further measurements, since a linear factor of 3.6 % per nm was determined between both evaluation methods, see Figure 3B.

EIS and LSPR measurements were carried out in parallel. The highest SNR (max. signal change divided by tripled standard deviation) was achieved at frequency of 100 kHz. The results are plotted in Figure 3C. In contrast to Figure 3A, the $|Z_{NaCl}|/|Z_{DI}|$ signal decreases non-linearly with increasing NaCl concentration, since the solution with 231 g/L NaCl reached the impedimetric signal saturation limit[35].

A

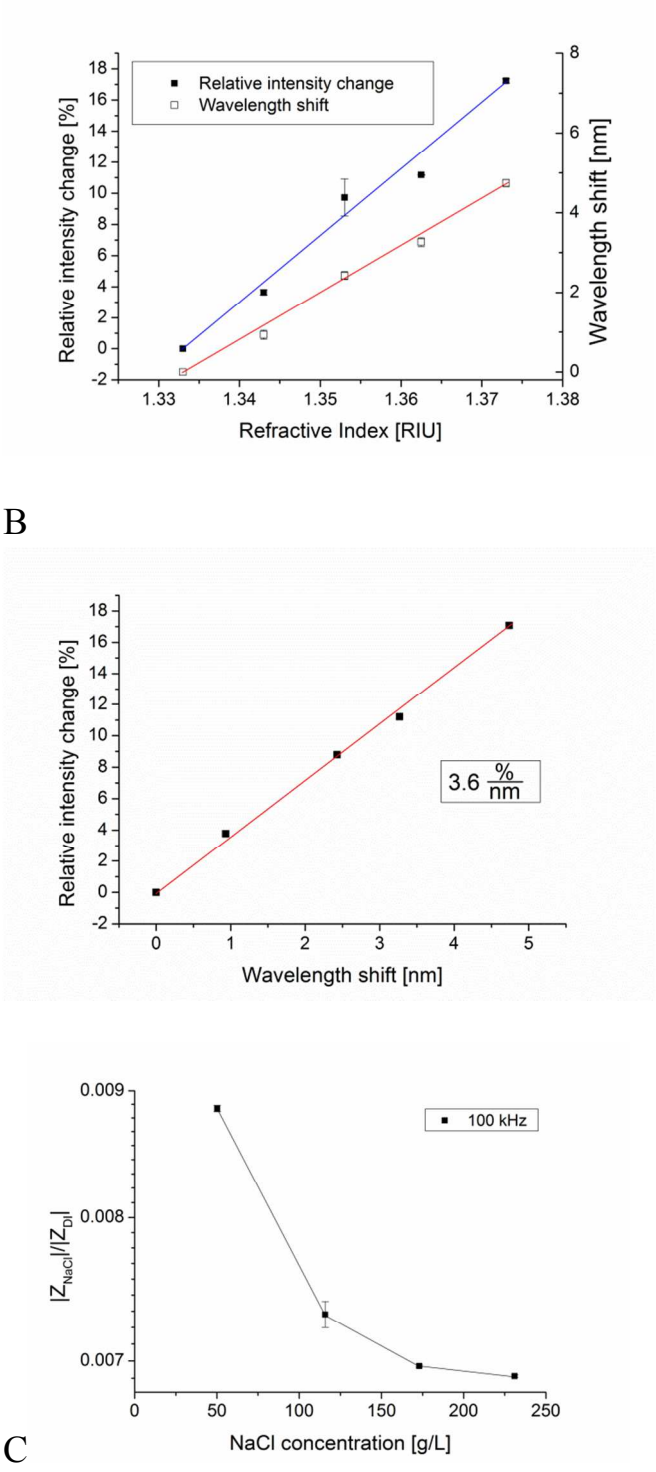

Figure 3: A) LSPR relative intensity change over refractive index of NaCl solutions with different concentrations. B) Linear relation between spectral barycentre relative intensity change and wavelength barycentre shift. C) Relative EIS amplitude signal over NaCl concentration measured at a frequency of 100 kHz. Error bars representing standard deviation appear at all measurements in figures A and C. Low values cannot be clearly displayed.

Sensor responses on fast bulk electrolyte switchovers were obtained by switching the medium from DI water to NaCl solution. In Figure 4A, the normalized impedance $|Z_{NaCl}|/|Z_{DI}|$ and the phase difference $\varphi_{DI} - \varphi_{NaCl}$ over the applied frequencies are plotted.

$|Z_{NaCl}|/|Z_{DI}|$ decreases with increasing frequency for all NaCl concentrations and show a minimum at around 40 kHz. The change in ion concentration has a large effect on the bulk resistivity which mainly contributes to the EIS signal at high frequencies. In contrast, the change of ion concentration has minimal influence on the electrical double layer in close vicinity to the electrodes. The electrical double layer contributes mainly to the EIS signal at low frequencies.

Phase differences form a typical RC-interaction peak at around 10 kHz, as shown in Figure 4A, but lacks on stability, as pointed out by the large error bars. Figure 4B represents time-resolved $|Z|/|Z_{NaCl}|$ signals measured at 1 Hz and 100 kHz for a medium switchover from DI water to NaCl solution, here with a concentration of 50.16 g/L. The relative intensity of the LSPR signal is included for comparison. The developments of the EIS signal at 1 Hz is comparable to the LSPR signal with settling time of 60 s, whereas EIS signal at 100 kHz settles already in 30 s. The response of the system on electrolyte changes without any adsorption effects has neither a lasting effect on the electrical double layer which contributes mainly to the signal at 1 Hz nor on the bulk resistivity which is the dominant input to the signal at 100 kHz. In comparison, the LSPR signal reacts according to the double-layer and shows similarity with the EIS signal observed at 1 Hz.

A

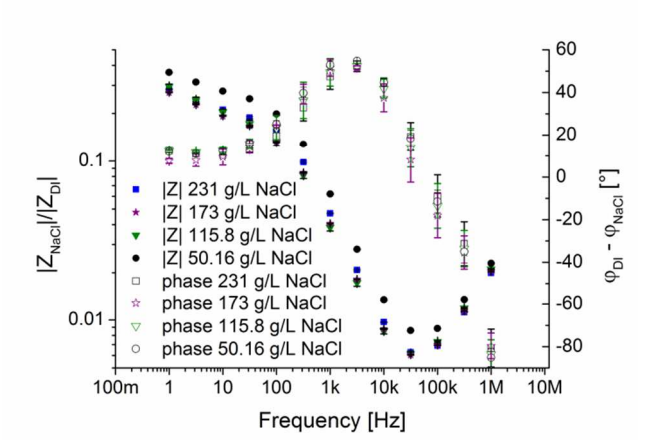

B

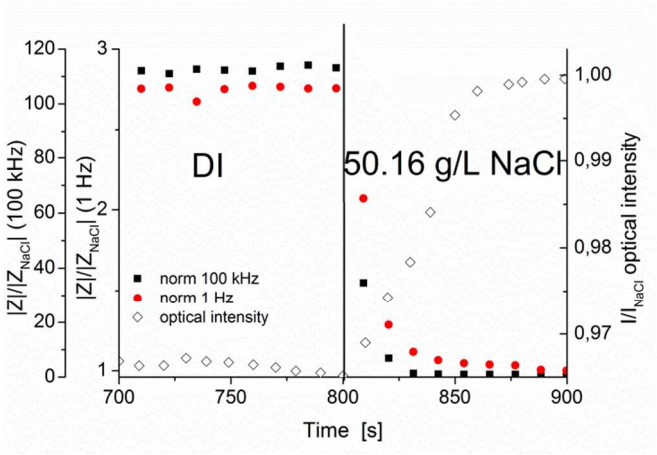

Figure 4: A) EIS amplitude ratio and EIS phase differences for a DI to NaCl solution switchover with respect to the applied frequencies. B) Time-resolved $|Z|/|Z_{NaCl}||$ signals measured at 1 Hz and 100 kHz for a medium switchover from DI water to NaCl solution, here with a concentration of 50.16 g/L. The relative intensity of the LSPR signal is included for comparison.

Non-specific protein binding was performed to characterize the reaction kinetics in a comparison of both, the LSPR and EIS method. BSA was chosen as a favorable candidate for its affinity to gold due to the thiol group on its surface and for the ability to form a thin monolayer with a height below 1 nm on the electrode surface[47,48]. The electrodes sputtered on the nano-porous membrane were consecutively treated with PBS, 1 % BSA in PBS followed by a PBS purge. Normalized impedance $|Z|/|Z_0|$ (Z_0 is the impedance signal of PBS level before 1 % BSA injection) and phase difference $\varphi_{DI} - \varphi_{PBS}$ with respect to frequency are shown in Fig. 5A. In general, EIS amplitude signals show higher sensitivities to BSA binding in the low frequency range which corresponds to changes of the electrical double layer. The lower sensitivities measured in the high frequency range can be correlated to minor changes of the bulk solution resistivity. Phase signals between 1 kHz and 100 kHz exhibit strong noise. Figure 5B demonstrates impressively that the time-dependent development of the LSPR signal corresponds more to the EIS signal at 100 kHz rather than to the impedance signal at 1 Hz. Although the slower rise time of the EIS 100 kHz signal compared to the LSPR signal indicates that certain portion of the signal comes from the total electrode surface, whereas the LSPR signal is mainly coming from the nanohole regions and is therefore faster. Thus, it can be concluded that LSPR is more sensitive to bulk solution effects at the pore region, whereas EIS at low frequencies is more sensitive to binding effects at the overall surface. This is based on the observation in Figure 5, where the EIS signal decreases less compared to the LSPR signal during the final PBS purge. This implies also that the origin of the LSPR signal contains information not only from the closest space of the electrode surface, here defined by the BSA monolayer, but is a combination of bulk refractive changes, molecular binding and changes of dielectric properties of the electrode metal film, as already discussed in[42]. Moreover, the LSPR signal originates from the events taking place on the edges of the nanoholes[49,50]. Here, the highest flow velocity is expected which explains the rather fast desorption of BSA indicated by the LSPR signal. At the holes, the average residence time of a BSA molecule is lower than over the area of the membrane. This leads to insufficient interaction with the gold, low binding, and fast desorption. In contrast, the EIS signals which are derived from the whole area of the membrane show less desorption or tighter binding. This is correlated to lower flow velocities over the total surface of the membrane.

A

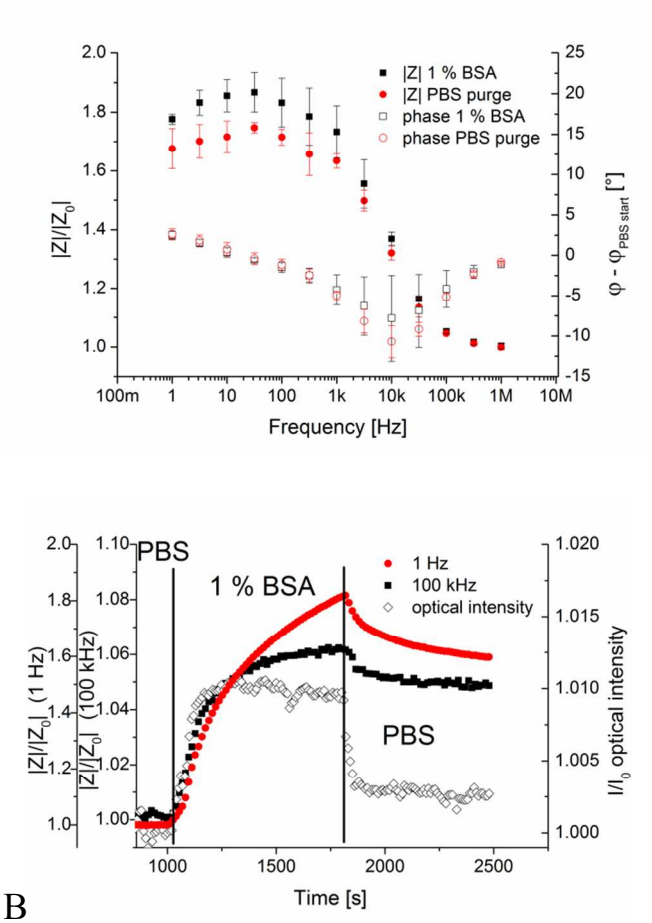

Figure 5: A) Normalized impedance amplitude $|Z|/|Z_0|$ (Z_0 is impedance signal of PBS level before 1 % BSA injection) and phase difference φ_{DI} - φ_{PBS} with respect to frequency. B) Time-resolved measurement of relative EIS amplitude at 1 Hz and 100 kHz during BSA adsorption. LSPR signals are added for comparison.

GLYCOPOLYMER - LECTIN BINDING

A more complex assay with variable thickness was used to show the dependency of the EIS and LSPR sensor outputs on the signal origins in more detail. The SI-ATRP process was performed on the electrodes resulting in 3.4 nm thick multivalent glycopolymer layer, as described in[15]. GS-II lectin binding assay was performed by consecutively injecting PBS buffer, 20 µg/ml of GS-II in PBS buffer and finally PBS buffer. Figure 6A shows the ratio of EIS amplitude signals Z/Z_0 with respect to time for different frequencies. Two different time response regimes were observed. At frequencies below 100 Hz GS-II binding but no significant desorption was observed, which can be assigned to optimum binding of lectin molecules to the glycopolymer brushes. The low frequency range corresponds mainly to the electrical double-layer and therefore to the polymer brush near the total electrode surface. In contrast, the GS-II binding signal is much slower at higher frequencies, where significant desorption is observed.

Kinetic constants were calculated using GraphPad Prism 6 evaluation software and summarized in Table 1. k_{on} values are in the common range for biomolecular interactions and prove together with the very low K_D values glycopolymer brushes as superb kind of ligand presentation for carbohydrate binding proteins. In general, with lectin K_D values in the mM range have been reported[51,52]. Here, the ligands are presented in a multivalent environment enhancing the avidity of the lectins dramatically. Remarkably, half-lifes of up to 80 h may be calculated from the k_{off} values. EIS reveals a significant increase in binding velocity with decreasing frequency as indicated by the k_{on} values. Interestingly, this is in contrast to our previous study with interdigitated EIS electrodes in a flow-over configuration[15]. The different behavior may be correlated to the more easily accessibility of the brushes to the glycans at the pores in the flow-through geometry where higher flow velocities and therefore brush deflections occur at the pore edges. The latter also explains the very fast binding kinetics reached in this setup, as the localized accessible multivalency is even higher at the pore surfaces than in the EIS setup with gold electrodes.

The time-resolved behavior of LSPR and EIS signals (see Figure 6 A and C) obtained from lectin binding is different compared to the behavior when BSA absorbs on the electrodes. Thickness related insulation of the electrode surface by covering the electrode surface with polymer brushes might be one reason. In addition, lectin binding takes place at larger distance from the surface as in the case of BSA which binds directly on the surface. The kinetic constants k_{on} for association and k_{off} for dissociation in Table 1 show the best conformity of LSPR and EIS signals at frequencies between 1 Hz and 10 Hz. The signal origin at these frequencies is closely related to the accessibility of sugar ligands by perturbation of the electrical double layer at the closest vicinity of the total electrode surface with slower flow conditions compared the nanoholes. The flow-through setup arrangement facilitates a fast and strong binding to the glycans reachable by deflection of the glycobrushes at the edges of the nanoholes, resulting in LSPR signals with very high k_{on} and low K_D values. In addition, diffusion effects do not really occur which are dominant in flow-over configurations. Therefore, the lectin shows strong and stable binding even at flow conditions due to very low k_{off} values. As shown above for BSA treatment, signal intensity of EIS decreases with increasing frequency, because the polymer layer weakens the signal like an insulator. However, lectin binding events at higher frequencies can be followed in EIS revealing very poor overall binding in the outer area of the glycopolymers brushes. This may indicate the dynamic desorption and rebinding of the lectin on its way through the polymer layer. Additionally, we recorded data with the 20 µg/ml lectin ECL from *Erythrina cristagalli* as negative control. ECL binds selectively to lactose residues and is not known to interact with GlcNAc moieties[53]. Interestingly, the LSPR (Fig. 6 C grey data) data show clearly that no binding occurs, whereas with EIS (Fig. 6 B) a binding signal is recorded. However, a complete desorption of the protein can be recognized at all frequencies after switching to buffer. This implies a weak non-specific interaction of ECL with the surface. To explain the clear absence of binding signal with LSPR compared to EIS we assume a non-specific interaction of ECL with the surface that is not strong enough to exist under flow conditions through the pores.

The signal origin of EIS at frequencies below 100 Hz is attributed to the total surface of the gold membrane where almost no flow occurs and proteins can settle down onto the surface. In contrast, the LSPR signal arises from the pore edges, the location of highest flow. The setup allows analyzing the binding behavior under flow-conditions (LSPR, EIS higher 100 Hz) as well as under static conditions (EIS, lower 100 Hz) at the same time. Static unspecific interaction of proteins with surfaces is well known from solid state assays like ELISA.

This means that our setup is a useful tool to analyze biomolecular interactions at the two mostly used flow conditions in one single measurement.

A

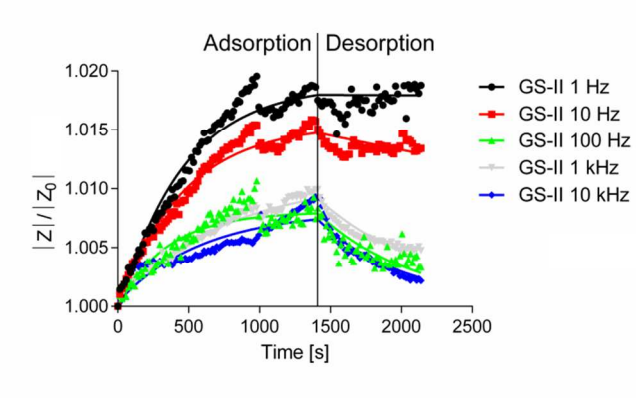

B

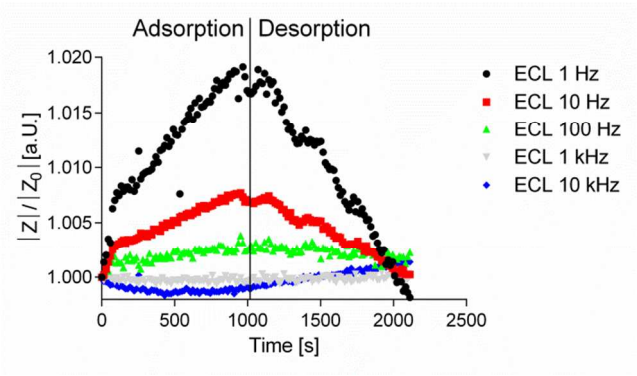

C

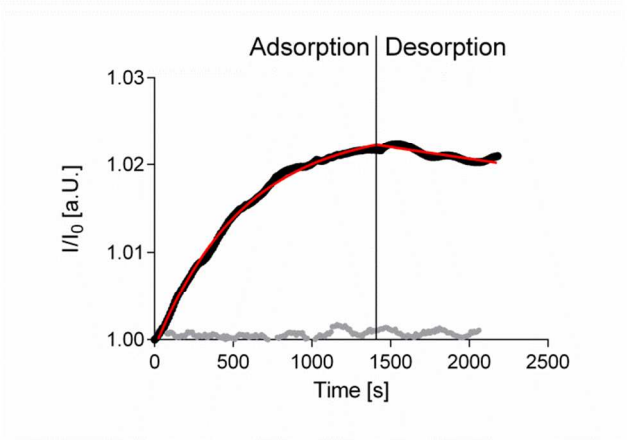

Figure 6: A) Time-resolved normalized EIS signal of lectin GS-II binding to glycopolymer brushes at frequencies between 1 Hz and 10 kHz. B) Time-resolved normalized EIS signal of ECL binding to glycopolymer brushes at frequencies between 1 Hz and 10 kHz as negative control. No specific interaction with the glycopoylmer brushes is detected as full desorption is recorded. C) Time-resolved normalized LSPR intensity signal of lectin binding on glycopolymer brushes (black with red fitting function) and binding of ECL to glycopolymers brushes as negative control (grey).

Table 1. k_{on}, k_{off} and K_D values determined from the data in Figure 6 for EIS and LSPR signals of frequencies between 1 Hz and 10 kHz.

Signal	k_{on} [$M^{-1}s^{-1}$]	k_{off} [s^{-1}]	$k_{off}/k_{on}=K_D$ [M]
1 Hz	1.5420E04	3.344E-06	2.169E-10
10 Hz	1.3783E04	1.760E-04	1.277E-08
100 Hz	1.0215E04	1.407E-03	1.378E-07
1 kHz	1.632E01	1.267E-03	7.765E-05
10 kHz	8.938E00	1.689E-03	1.890E-05
LSPR	1.5870E04	1.390E-04	8.784E-09

CONCLUSIONS

A novel combined EIS – LSPR based microfluidic flow-through sensor was developed and tested. A very fast signal response to molecule binding on the sensor surface was demonstrated for both measurement methods. BSA adsorption and GS-II lectin binding show specific binding kinetics in dependency on the applied frequency. Changes in the bulk solution can be observed in EIS data over time at frequencies above 10 kHz, whereas binding effects exhibit signal changes at frequencies below 1 kHz. The LSPR signal can be described by a combination of both bulk and binding parts of the signal. It was shown that the time resolved LSPR signal of thin BSA monolayer adhesion (thickness below 1 nm) have more similarity with the EIS high frequency signal which is influenced rather by bulk than by low frequency signal correlated to the electrical double layer. The LSPR signals of GS-II lectin binding to glycopolymer brushes layer with thickness of 3.4 nm provide significant agreement with EIS signals obtained at low frequencies. This confirms that the thickness of the electrode coverage has an impact on the LSPR signal. When using only LSPR there is no possibility to differentiate the signal contribution coming from surface-near and surface far. The combination of LSPR and EIS offers a unique possibility to specify the origin of the signal. Moreover, by including measurements of non-binder ECL, we monitored very different behavior of LSPR and EIS signals. We can conclude that our system is capable of measuring biomolecular binding events under flow- as well as static conditions in one single analysis. This makes our system a very versatile biosensor. Both, ELISA-like assays and SPR-assays can now be performed at once and with minimal effort to get in-depth understanding of biomolecular binding events. Additionally, the scope of this system may be broadened by changing the ligands or tuning the polymer to serve as scaffold for all kind of ligand presentation besides glycans.

ASSOCIATED CONTENT

AUTHOR INFORMATION

Corresponding Author

*Uwe Schnakenberg (schnakenberg@iwe1.rwth-aachen.de)

Present Addresses

Dr. Ruben R. Rosencrantz: Fraunhofer Institute for Applied Polymer Research (IAP), Geiselbergstraße 69, 14476 Potsdam, Germany

Notes

The authors declare no competing financial interest.

Author Contributions

The manuscript was written through contributions of all authors. All authors have given approval to the final version of the manuscript.

ACKNOWLEDGMENT

The authors express their sincere thanks to Mr. Thomas Keutgens for carrying out LSPR and EIS experiments and to Dr. Hyunji Park for deposition of glycopolymers. The authors thank Prof. Dr. Alexander Böker for ongoing support and helpful discussions.

REFERENCES

(1) van Gerwen, P.; Laureyn, W.; Laureys, W.; Huyberechts, G.; Beeck, M. op de; Baert, K.; Suls, J.; Sansen, W.; Jacobs, P.; Hermans, L., et al., *Sens. Actuators, B.* **1998**, *49,* 73–80.

(2) Li, A.; Yang, F.; Ma, Y.; Yang, X., *Biosens. Bioelectron.* **2007**, *22,* 1716–1722.

(3) Fu, Y.; Yuan, R.; Xu, L.; Chai, Y.; Zhong, X.; Tang, D., *Biochem. Eng. J.* **2005**, *23,* 37–44.

(4) Wang, R.; Wang, Y.; Lassiter, K.; Li, Y.; Hargis, B.; Tung, S.; Berghman, L.; Bottje, W., *Talanta.* **2009**, *79,* 159–164.

(5) Lum, J.; Wang, R.; Lassiter, K.; Srinivasan, B.; Abi-Ghanem, D.; Berghman, L.; Hargis, B.; Tung, S.; Lu, H.; Li, Y., *Biosens. Bioelectron.* **2012**, *38,* 67–73.

(6) Heiskanen, A. R.; Spégel, C. F.; Kostesha, N.; Ruzgas, T.; Emnéus, J., *Langmuir.* **2008**, *24,* 9066–9073.

(7) Sun, T.; Gawad, S.; Bernabini, C.; Green, N. G.; Morgan, H., *Meas. Sci. Technol.* **2007**, *18,* 2859–2868.

(8) Holmes, D.; Pettigrew, D.; Reccius, C. H.; Gwyer, J. D.; van Berkel, C.; Holloway, J.; Davies, D. E.; Morgan, H., *Lab Chip.* **2009**, *9,* 2881–2889.

(9) Morgan, H.; Sun, T.; Holmes, D.; Gawad, S.; Green, N. G., *J. Phys. D: Appl. Phys.* **2007**, *40,* 61–70.

(10) Lvovich, V. F. *Impedance spectroscopy. Applications to electrochemical and dielectric phenomena;* Wiley: Hoboken, N.J, 2012.

(11) Franks, W.; Schenker, I.; Schmutz, P.; Hierlemann, A., *IEEE Trans Biomed Eng.* **2005**, *52,* 1295–1302.

(12) Shrikrishnan, S.; Sankaran, K.; Lakshminarayanan, V., *J. Phys. Chem. C.* **2012**, *116,* 16030–16037.

(13) Jagadeesh, R. V.; Lakshminarayanan, V., *Electrochim. Acta.* **2016**, *197,* 1–9.

(14) Park, H.; Rosencrantz, R. R.; Elling, L.; Böker, A., *Macromol. Rapid Commun.* **2015**, *36,* 45–54.

(15) Lazar, J.; Park, H.; Rosencrantz, R. R.; Böker, A.; Elling, L.; Schnakenberg, U., *Macromol. Rapid Commun.* **2015**, *36,* 1472–1478.

(16) Kretschmann, E.; Raether, H., *Z. Naturforsch. A.* **1968**, *23,* 2135–2136.

(17) Homola, J., *Chem. Rev.* **2008**, *108,* 462–493.

(18) Squires, T. M.; Messinger, R. J.; Manalis, S. R., *Nat Biotechnol.* **2008**, *26,* 417–426.

(19) Ebbesen, T. W.; Lezec, H. J.; Ghaemi, H. F.; Thio, T.; Wolff, P. A., *Nature.* **1998**, *391,* 667–669.

(20) Thio, T.; Ghaemi, H. F.; Lezec, H. J.; Wolff, P. A.; Ebbesen, T. W., *J. Opt. Soc. Am. B.* **1999**, *16,* p. 1743.

(21) Sharpe, J. C.; Mitchell, J. S.; Lin, L.; Sedoglavich, N.; Blaikie, R. J., *Anal. Chem.* **2008**, *80,* 2244–2249.

(22) Eftekhari, F.; Escobedo, C.; Ferreira, J.; Duan, X.; Girotto, E. M.; Brolo, A. G.; Gordon, R.; Sinton, D., *Anal. Chem.* **2009**, *81,* 4308–4311.

(23) Yanik, A. A.; Huang, M.; Artar, A.; Chang, T.-Y.; Altug, H., *Appl. Phys. Lett.* **2010**, *96,* p. 21101.

(24) Escobedo, C.; Brolo, A. G.; Gordon, R.; Sinton, D., *Anal. Chem.* **2010**, *82,* 10015–10020.

(25) Cetin, A. E.; Coskun, A. F.; Galarreta, B. C.; Huang, M.; Herman, D.; Ozcan, A.; Altug, H., *Light Sci Appl.* **2014**, *3,* e122.

(26) Escobedo, C.; Vincent, S.; Choudhury, A. I. K.; Campbell, J.; Brolo, A. G.; Sinton, D.; Gordon, R., *J. Micromech. Microeng.* **2011**, *21,* p. 115001.

(27) Escobedo, C.; Brolo, A. G.; Gordon, R.; Sinton, D., *Nano Lett.* **2012**, *12,* 1592–1596.

(28) Fan, M.; Thompson, M.; Andrade, M. L.; Brolo, A. G., *Anal. Chem.* **2010**, *82,* 6350–6352.

(29) Gao, H.; Hyun, J. K.; Lee, M. H.; Yang, J.-C.; Lauhon, L. J.; Odom, T. W., *Nano Lett.* **2010**, *10,* 4111–4116.

(30) Kan, T.; Matsumoto, K.; Shimoyama, I., *J. Micromech. Microeng.* **2010**, *20,* p. 85032.

(31) Ye, J.; Wen, F.; Sobhani, H.; Lassiter, J. B.; van Dorpe, P.; Nordlander, P.; Halas, N. J., *Nano Lett.* **2012**, *12,* 1660–1667.

(32) Chen, S.; Svedendahl, M.; van Duyne, R. P.; Käll, M., *Nano Lett.* **2011**, *11,* 1826–1830.

(33) Buchenauer, A.; Bialon, M.; Segun, D.; Püttmann, C.; Stein, C.; Barth, S.; Schnakenberg, U., *J. Micromech. Microeng.* **2014**, *24,* p. 34001.

(34) Rosencrantz, R. R.; Nguyen, V. H.; Park, H.; Schulte, C.; Boker, A.; Schnakenberg, U.; Elling, L., *Anal. Bioanal. Chem.* **2016**, *408,* 5633–5640.

(35) Patskovsky, S.; Latendresse, V.; Dallaire, A.-M.; Doré-Mathieu, L.; Meunier, M., *Analyst.* **2014**, *139,* 596–602.

(36) Hong, B.; Sun, A.; Pang, L.; Venkatesh, A. G.; Hall, D.; Fainman, Y., *Opt. Express.* **2015**, *23,* 30237–30249.

(37) Vandenryt, T.; Pohl, A.; van Grinsven, B.; Thoelen, R.; Ceuninck, W. de; Wagner, P.; Opitz, J., *Sensors (Basel, Switzerland).* **2013**, *13,* 14650–14661.

(38) Wu, C.; Rehman, F. u.; Li, J.; Ye, J.; Zhang, Y.; Su, M.; Jiang, H.; Wang, X., *ACS Appl. Mater. Interfaces.* **2015**, *7,* 24848–24854.

(39) Cheng, X. R.; Hau, B. Y. H.; Endo, T.; Kerman, K., *Biosens. Bioelectron.* **2014**, *53,* 513–518.

(40) Shan, X.; Patel, U.; Wang, S.; Iglesias, R.; Tao, N., *Science.* **2010**, *327,* 1363–1366.

(41) Foley, K. J.; Shan, X.; Tao, N. J., *Anal. Chem.* **2008**, *80,* 5146–5151.

(42) Wang, S.; Huang, X.; Shan, X.; Foley, K. J.; Tao, N., *Anal. Chem.* **2010**, *82,* 935–941.

(43) Lu, J.; Wang, W.; Wang, S.; Shan, X.; Li, J.; Tao, N., *Anal. Chem.* **2012**, *84,* 327–333.

(44) Polonschii, C.; David, S.; Gáspár, S.; Gheorghiu, M.; Rosu-Hamzescu, M.; Gheorghiu, E., *Anal. Chem.* **2014**, *86,* 8553–8562.

(45) Lazar, J.; Schnelting, C.; Slavcheva, E.; Schnakenberg, U., *Anal. Chem.* **2016**, *88,* 682–687.

(46) Yunus, W. Mahmood bin Mat; Rahman, A. b. A., *Appl. Opt.* **1988**, *27,* p. 3341.

(47) Phan, H. T. M.; Bartelt-Hunt, S.; Rodenhausen, K. B.; Schubert, M.; Bartz, J. C.; Hinderberger, D., *PLoS ONE.* **2015**, *10,* e0141282.

(48) Chen, H.; Kim, Y. S.; Lee, J.; Yoon, S. J.; Lim, D. S.; Choi, H.-J.; Koh, K., *Sensors.* **2007**, *7,* 2263–2272.

(49) Çetin, A. E.; Yanik, A. A.; Yilmaz, C.; Somu, S.; Busnaina, A.; Altug, H., *Appl. Phys. Lett.* **2011**, *98,* p. 111110.

(50) Lalanne, P.; Hugonin, J. P.; Rodier, J. C., *Phys. Rev. Lett.* **2005**, *95,* p. 263902.

(51) Rachel, H.; Chang-Chun, L., *Adv. Carbohydr. Chem. Biochem.* **2013**, *69,* 125–207.

(52) Dam, T. K.; Cavada, B. S.; Grangeiro, T. B.; Santos, C. F.; Ceccatto, V. M.; Sousa, F. A. de; Oscarson, S.; Brewer, C. F., *J. Biol. Chem.* **2000**, *275,* 16119–16126.

(53) Turton, K.; Natesh, R.; Thiyagarajan, N.; Chaddock, J. A.; Acharya, K. R., *Glycobiology.* **2004**, *14,* 923–929.

ToC graphic

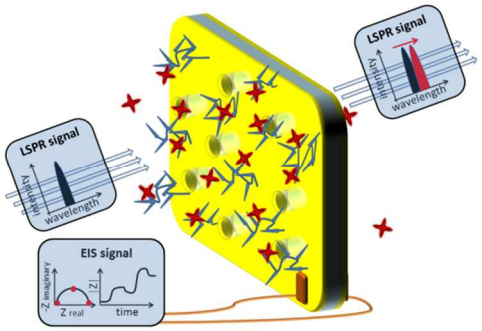
LSPR signal
intensity
wavelength
LSPR signal
intensity
wavelength
EIS signal
-Z imaginary
Z real
Z
time

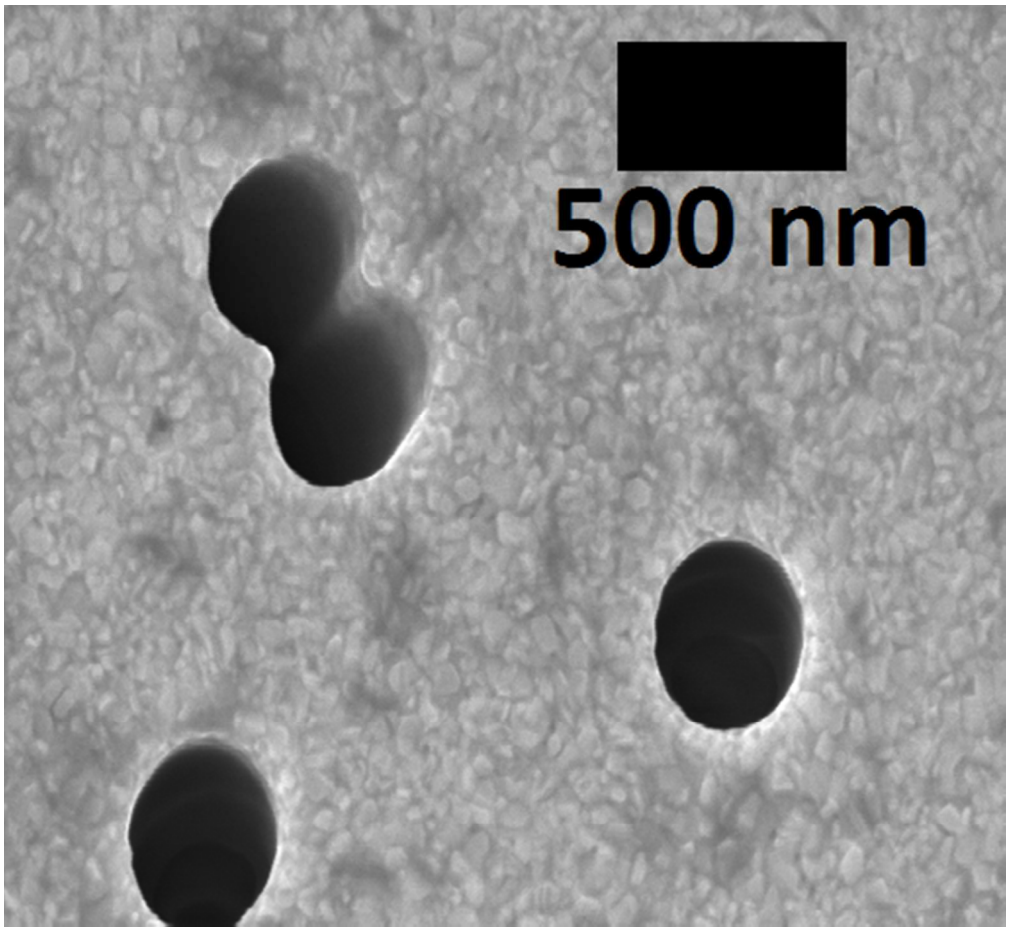

Figure 1: SEM image, top view of sputtered membrane showing nanoholes with straight inner walls.

135x124mm (96 x 96 DPI)

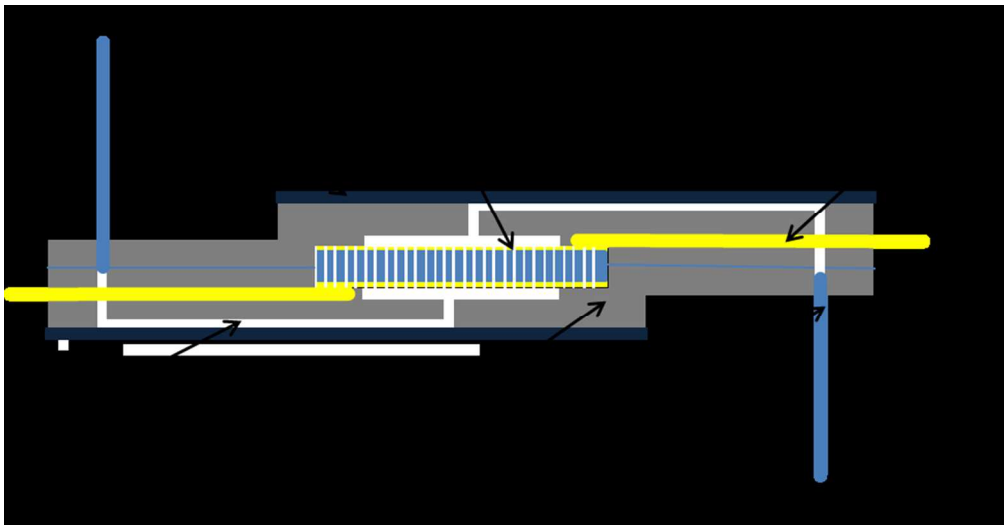

Figure 2: A) Scheme of the PDMS microfluidic system with clamped membrane. B) Schematic block diagram of the whole measurement setup. A) and B) not to scale.

164x85mm (150 x 150 DPI)

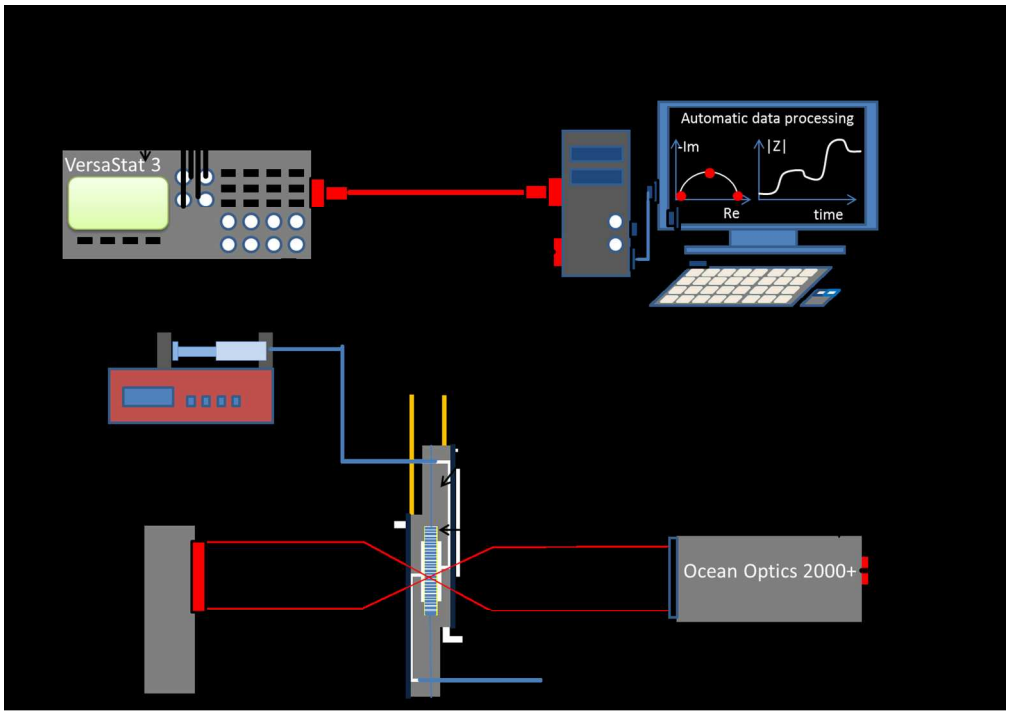

Figure 2: A) Scheme of the PDMS microfluidic system with clamped membrane. B) Schematic block diagram of the whole measurement setup. A) and B) not to scale.

265x187mm (150 x 150 DPI)

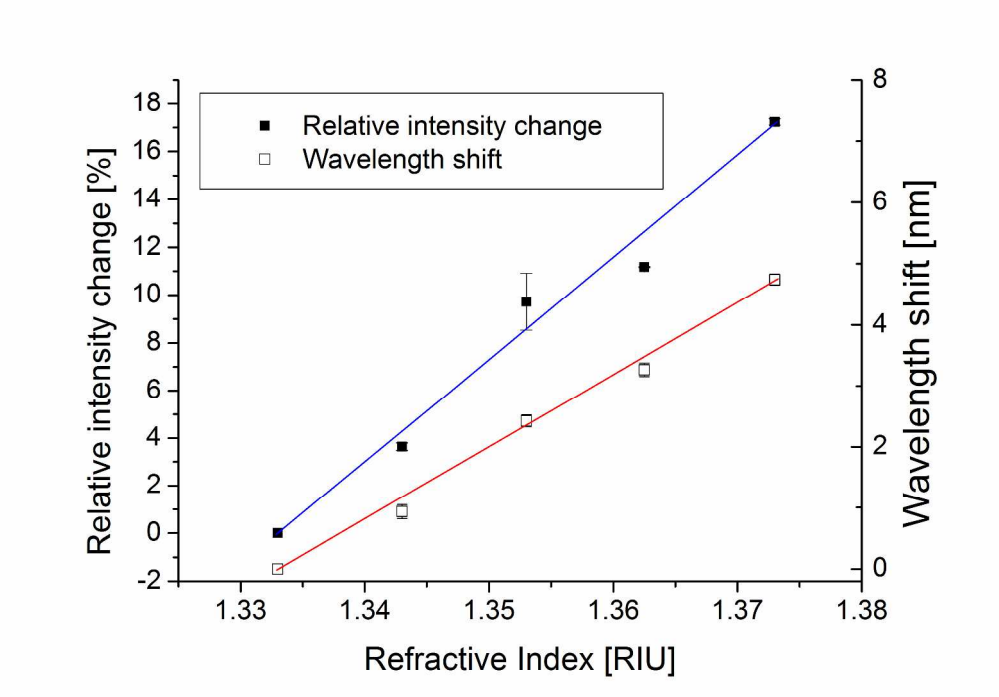

Figure 3: A) LSPR relative intensity change over refractive index of NaCl solutions with different concentrations. B) Linear relation between spectral barycentre relative intensity change and wave-length barycentre shift. C) Relative EIS amplitude signal over NaCl concentration measured at a frequency of 100 kHz. Error bars standing for standard deviation appear at all measurements in figures A and C. Low values cannot be clearly displayed.

288x201mm (300 x 300 DPI)

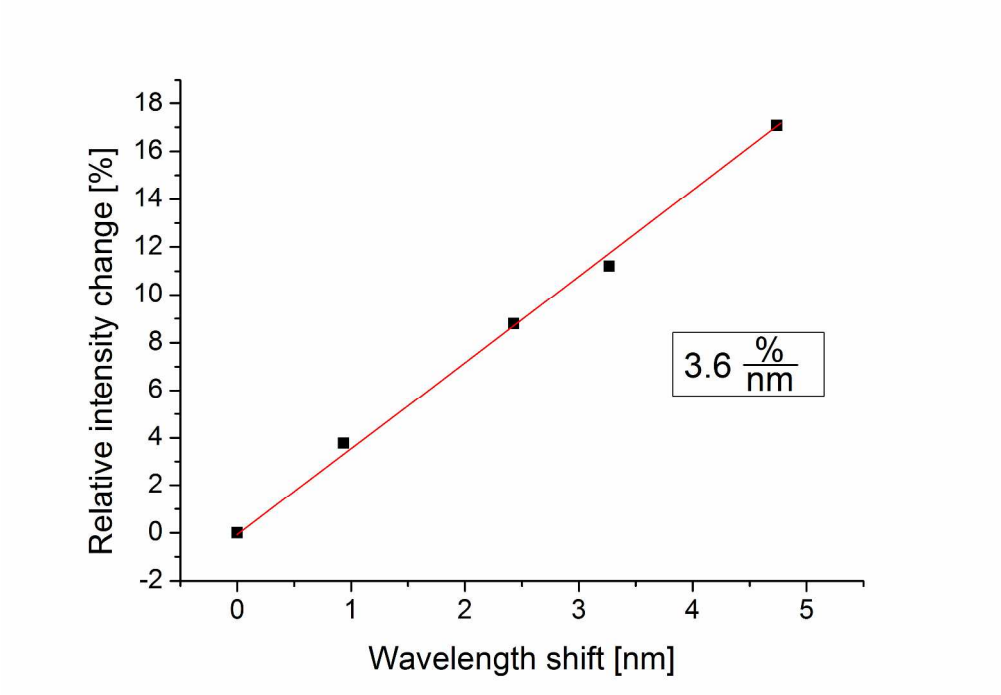

Linear relation between spectral barycentre relative intensity change and wavelength barycentre shift.

288x201mm (300 x 300 DPI)

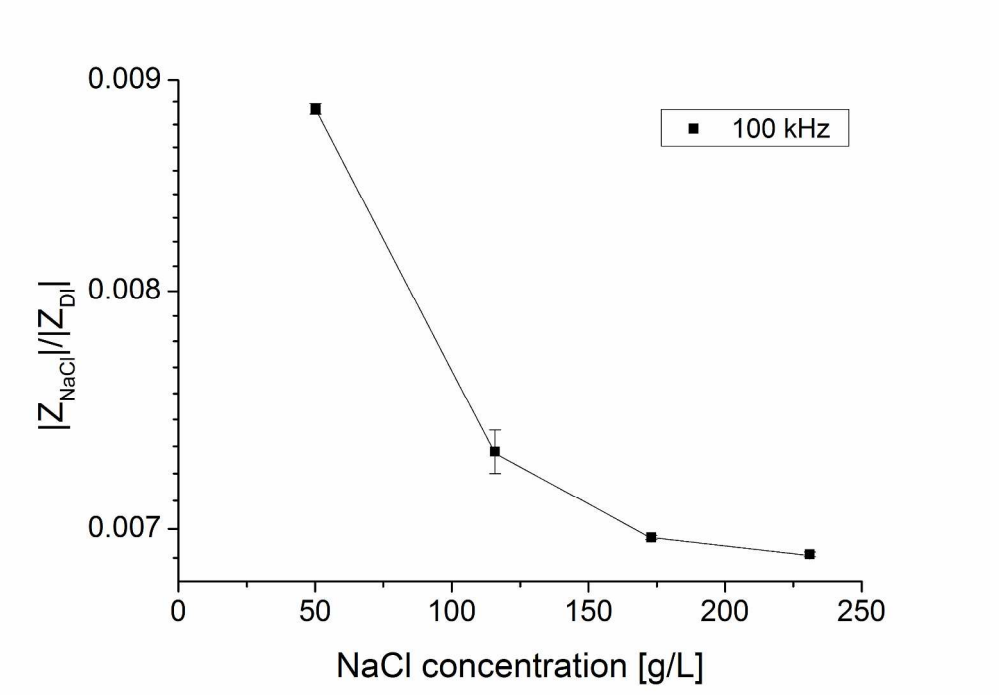

Relative EIS amplitude signal over NaCl concentration measured at a frequency of 100 kHz. Error bars representing standard deviation appear at all measurements in figures A and C. Low values cannot be clearly displayed.

288x201mm (300 x 300 DPI)

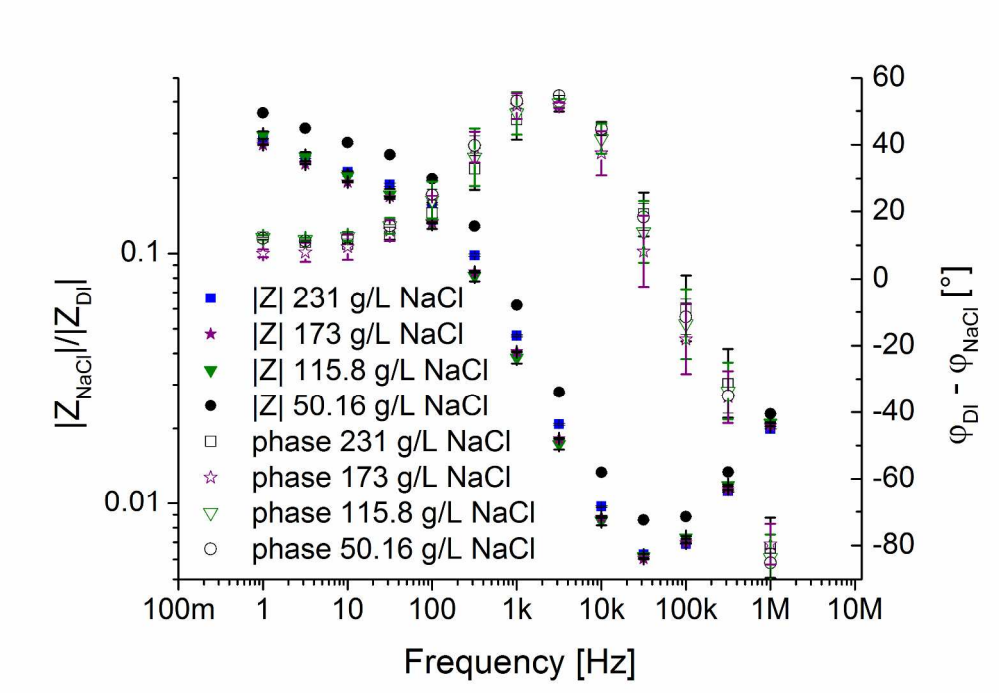

EIS amplitude ratio and EIS phase differences for a DI to NaCl solution switchover with respect to the applied frequencies.

288x201mm (300 x 300 DPI)

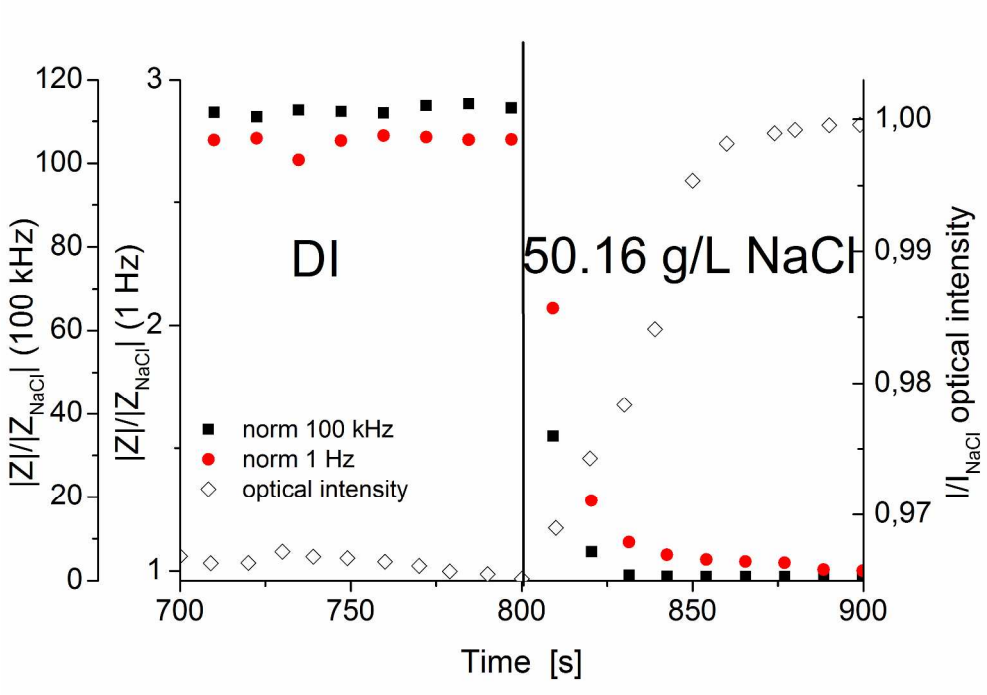

Time-resolved |Z| /|ZNaCl|| signals measured at 1 Hz and 100 kHz for a medium switchover from DI water to NaCl solution, here with a concentration of 50.16 g/L. The relative intensity of the LSPR signal is included for comparison.

288x201mm (300 x 300 DPI)

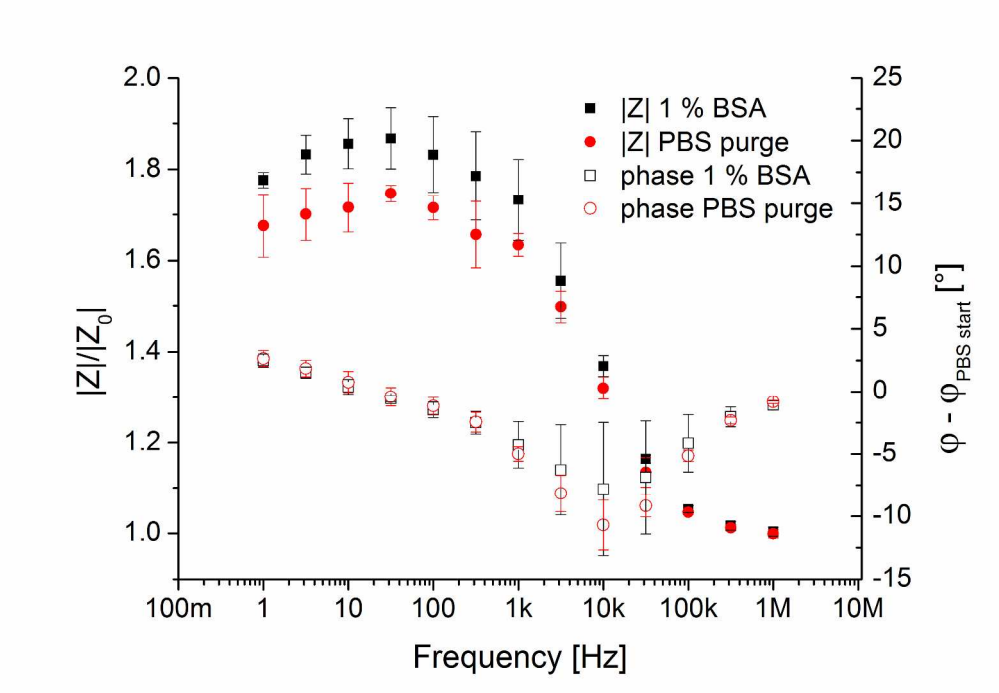

Normalized impedance amplitude |Z|/|Z0| (Z0 is impedance signal of PBS level before 1 % BSA injection) and phase difference φDI - φPBS with respect to frequency.

288x201mm (300 x 300 DPI)

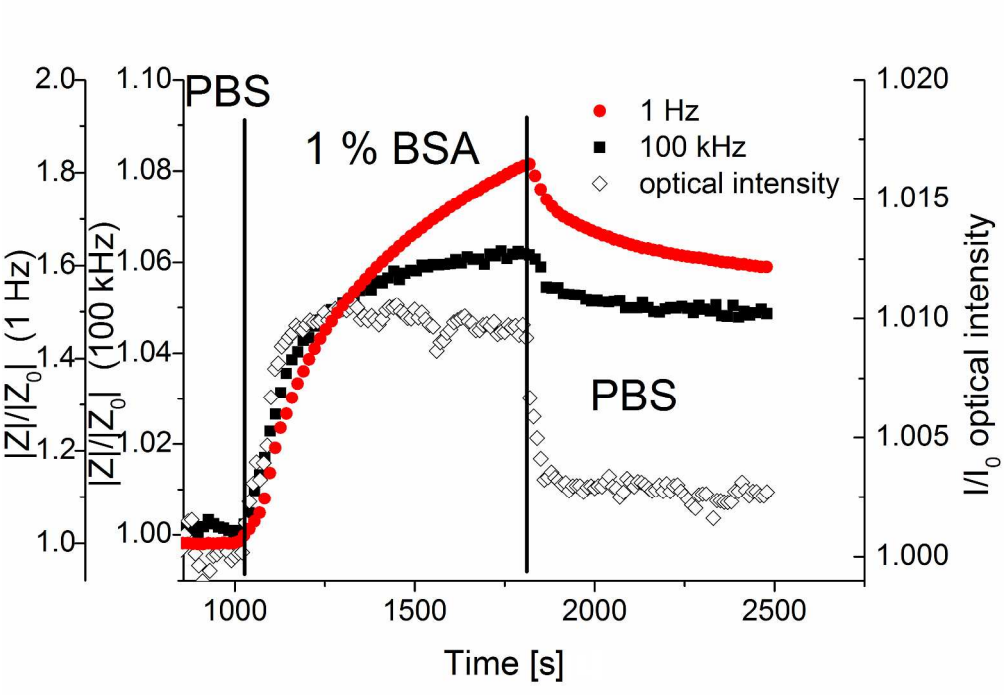

Time-resolved measurement of relative EIS amplitude at 1 Hz and 100 kHz during BSA adsorption. LSPR signals are added for comparison.

901x629mm (96 x 96 DPI)

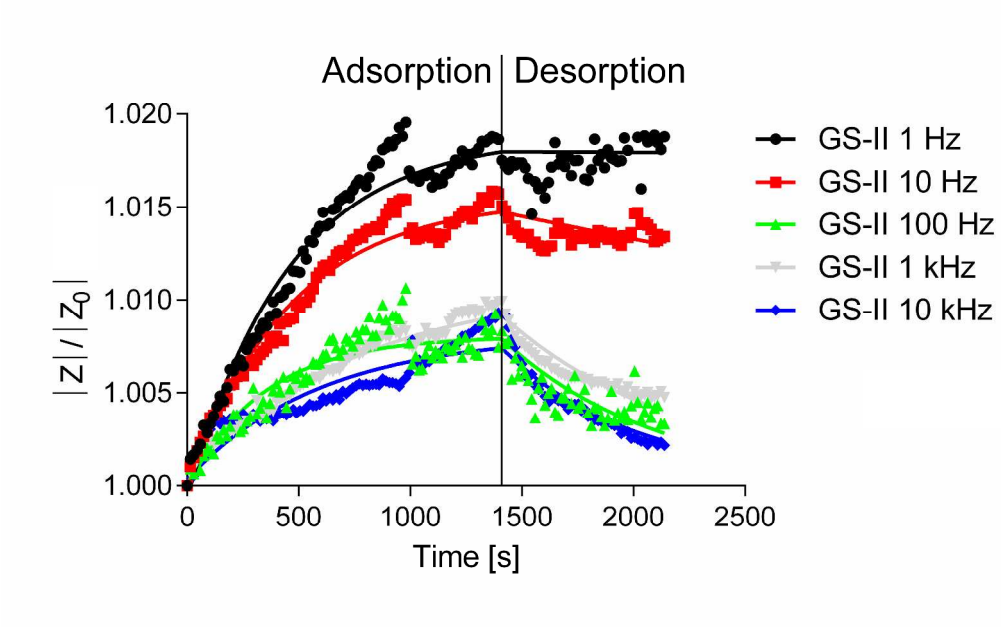

Time-resolved normalized EIS signal of lectin GS-II binding to glycopolymer brushes at frequencies between 1 Hz and 10 kHz.

1712x1075mm (96 x 96 DPI)

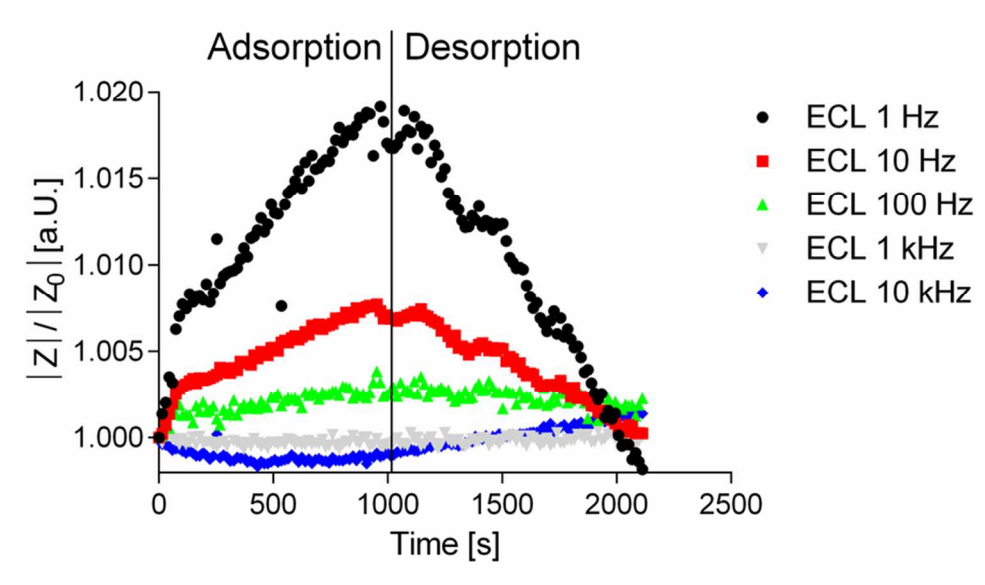

Time-resolved normalized EIS signal of ECL binding to glycopolymer brushes at frequencies between 1 Hz and 10 kHz as negative control. No specific interaction with the glycopoylmer brushes is detected as full desorption is recorded.

78x46mm (300 x 300 DPI)

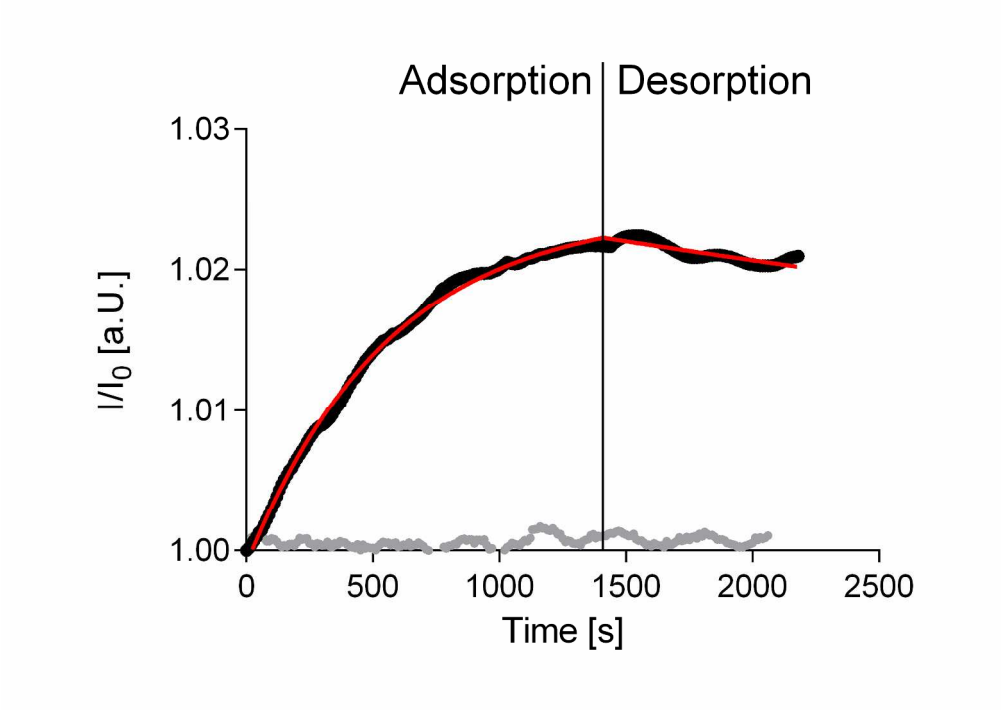

Time-resolved normalized LSPR intensity signal of lectin binding on glycopolymer brushes (black with red fitting function) and binding of ECL to glycopolymers brushes as negative control (grey).

753x537mm (96 x 96 DPI)